LIMNOLOGY and OCEANOGRAPHY

Hydrology drives export and composition of carbon in a pristine tropical river

Travis W. Drake [1]*, Matti Barthel,[1] Christian Ekemba Mbongo,[2] Davin Mata Mpambi,[3]
Simon Baumgartner,[4,5] Clement Ikene Botefa,[3] Marijn Bauters,[6] Martin R. Kurek,[7] Robert G. M. Spencer,[7]
Amy M. McKenna [8,9] Negar Haghipour,[10,11] Godé Lompoko Ekamba,[3] Jose N. Wabakanghanzi,[12]
Timothy I. Eglinton,[10] Kristof Van Oost,[4] Johan Six[1]

[1]Department of Environmental Systems Science, ETH Zürich, Zurich, Switzerland
[2]Coordination Provinciale de l'Environnement Equateur, Mbandaka, Democratic Republic of Congo
[3]Institute Congolais pour la Conservation de la Nature, Mbandaka, Democratic Republic of Congo
[4]Earth and Life Institute, Université Catholique de Louvain, Louvain-la-Neuve, Belgium
[5]Research Division Agroecology and Environment, Agroscope, Zurich, Switzerland
[6]Department of Green Chemistry and Technology, Ghent University, Ghent, Belgium
[7]Department of Earth, Ocean and Atmospheric Science, Florida State University, Tallahassee, Florida, USA
[8]National High Magnetic Field Laboratory, Florida State University, Tallahassee, Florida, USA
[9]Department of Soil and Crop Sciences, Colorado State University, Fort Collins, Colorado, USA
[10]Department of Earth Sciences, ETH Zurich, Zurich, Switzerland
[11]Laboratory for Ion Beam Physics, Department of Physics, ETH Zurich, Zurich, Switzerland
[12]Department of Soil Physics and Hydrology, Congo Atomic Energy Commission, Kinshasa, Democratic Republic of Congo

ABSTRACT

The Ruki is a pristine blackwater tributary in the Congo Basin draining tropical lowland forest. Daily discharge and fortnightly concentrations, isotopic ratios, and molecular composition of carbon and organic matter were measured for 1 yr (2019–2020). Like the Congo River, discharge peaked from November–January, with a smaller secondary peak in June. Dissolved organic carbon (DOC), inorganic carbon (DIC), carbon dioxide (pCO_2), and methane (pCH_4) concentrations were high (21.3 ± 4.8 mg C L^{-1}, 5.8 ± 0.9 mg C L^{-1}, 6370 ± 1740 ppm, and 250 ± 100 ppm, respectively) and positively correlated with discharge, indicating transport limitation. Total suspended solids and particulate organic carbon (POC) concentrations were generally low (3.68 ± 1.61 mg L^{-1}, 0.88 ± 0.33 mg C L^{-1}, respectively) and varied inversely with discharge, indicating source limitation. The Ruki exported a total of 3.25 Tg C yr^{-1}, of which DOC, DIC, and POC comprised 76%, 20%, and 3%, respectively. This DOC flux represents ∼ 20% of the annual Congo Basin flux from about 5% of its area, highlighting the high yield. Isotopic ratios of DOC and POC indicate modern C3 forest vegetation as a source, except for a few older samples potentially indicating peat inputs. The bulk molecular composition of dissolved organic matter was seasonally consistent; however, a more oxidized and aromatic assemblage occurred at high discharge, corresponding with forest vegetation, while a more aliphatic, nitrogen-, and sulfur-enriched assemblage was found during low discharge, corresponding with soil-derived organic matter. Overall, these results underscore how hydrology controls C concentrations in the Ruki River and how this blackwater river contributes disproportionately to C export per unit area within the Congo Basin hydrosystem.

*Correspondence: *draketw@gmail.com

Additional Supporting Information may be found in the online version of this article.

Author Contribution Statement: T.W.D., J.S., K.V.O., M. Barthel, S.B., and M. Bauters conceived of the study. T.W.D., M. Barthel, C.E.M., D.M.M., S.B., C.I.B., and M. Bauters conducted the fieldwork. M.K., R.G.M.S., and A.M.M. facilitated and performed the high-resolution mass spectrometry analyses. N.H. and T.I.I. facilitated and performed the carbon isotope analyses. G.L.E. and J.N.W. facilitated on-the-ground logistics and sampling site selection. M. Barthel, M. Bauters, S.B., R.G.M.S., M.K., J.S., and K.V.O. assisted T.W.D. in the drafting of the manuscript. All co-authors provided substantive revisions to the manuscript.

On a global scale, tropical rivers are major processors and conduits of carbon (C) to both the atmosphere and ocean. In the tropics, generally high rates of terrestrial productivity combined with high annual precipitation result in large fluxes of organic and inorganic C to and through the aquatic network relative to temperate ecosystems (Meybeck 1982). As a result, these aquatic fluxes can represent major components of terrestrial net ecosystem productivity and large transfers of reduced C downstream (Battin et al. 2009; Drake et al. 2018*b*). Constraining these fluxes and integrating them into terrestrial budgets (e.g., those derived from eddy-covariance or biomass inventories) are necessary tasks for reconciling basin-scale C balances and deriving accurate C sink estimates. This is particularly important for humid tropical forests, which are touted as vital sinks for atmospheric CO_2 despite research that has shown that at least some of this terrestrial sink is offset by aquatic CO_2 fluxes, depending on the proportion of CO_2 supplied by wetlands (Richey et al. 2002; Abril et al. 2014).

The Congo River Basin of central Africa drains a diverse 3.6 million km^2 of lowland forests, forest-savannah mosaics, savannah woodlands, and swamp forests. This massive tropical basin is the second largest supplier of freshwater and terrestrial dissolved organic carbon (DOC) to the ocean after the Amazon (Coynel et al. 2005; Raymond and Spencer 2015; Spencer et al. 2016). Most of the water and organic carbon (OC) that comprise this flux are sourced from the humid lowland forests that lie within the center of the Basin (Coynel et al. 2005; Spencer et al. 2016). So far, biogeochemical studies have primarily focused on assessing fluxes from the main stem of the Congo River at Kinshasa-Brazzaville (Coynel et al. 2005; Seyler et al. 2005; Wang et al. 2013; Lambert et al. 2016; Spencer et al. 2016; Hemingway 2017; Kurek et al. 2022). Previous studies have examined transects along Congo mainstem that included outlets of major tributaries (Lambert et al. 2016; Borges et al. 2019), the Oubangui River (Bouillon et al. 2012, 2014), the Kasai River (Borges et al. 2019), the Ngoko-Sangha River (Coynel et al. 2005), and smaller rivers of western (Mann et al. 2014; Upstill-Goddard et al. 2017; Drake et al. 2020*a*) and eastern Congo (Spencer et al. 2010; Drake et al. 2019; Baumgartner et al. 2022). While important, the main-stem studies are hindered by low temporal resolution and ambiguity arising from the convolution of fluxes and signals from multiple tributaries that drain different land covers. No studies to date have examined the fluxes nor seasonal composition of C from the Ruki River, a nearly completely pristine left-bank tributary to the Congo River representing a pure lowland forest endmember. The Ruki drains 188,800 km^2 of broadleaf and lowland swamp forests, with only minimal areas affected by agricultural conversion to croplands ($\sim 5\%$ of watershed area). As such, the Ruki is a good candidate for being one of the most pristine and homogeneous large tropical watersheds on Earth.

Large quantities of peat underlie much of the hardwood and palm-dominated swamp forests of the *Cuvette Centrale* depression of the Congo Basin (Dargie et al. 2017, 2019). Recent follow-up mapping efforts in the Democratic Republic of Congo have verified large tracts of river-influenced peat complexes in the Ruki Basin, highlighting the areas adjacent to the river channel as important locations of peat (Crezee et al. 2022). While some of the *Cuvette* peat complex lies within protected areas or areas designated as "Wetlands of International Importance" according to the Ramsar Convention (Dargie et al. 2019), it is yet unclear how these areas will be actively protected. Meanwhile, the peat complex is still threatened by climate and land-use change. Reduced rainfall, higher evapotranspiration, changes in rainfall timing, drainage for agriculture, and logging can all lead to the drying and enhanced decomposition of peat (Dargie et al. 2019). So far, the effect of climate change on regional precipitation is not well defined and most land-use change is confined to areas of *terra firme* forest, suggesting minimal peat degradation at present (Dargie et al. 2019). Nevertheless, the future stability of this long-term OC reservoir in the wake of climate and land-use change has important ramifications for the net C balance of the Congolese tropical forest system.

The source and composition of OC in a river can provide important information for the C cycle and landscape-level processes that occur within a basin. To that end, the proliferation and application of isotope ratio, accelerator, and Fourier-transform ion cyclotron resonance mass spectrometry have opened the door to characterizing and revealing the sources of C in rivers with a high degree of specificity. For example, stable carbon isotopic ratios can elucidate whether OC is sourced from C3 vs. C4 photosynthetic pathways (given their different fractionation rates) while radiocarbon can be used to identify contributions from modern vs. aged reservoirs such as soils or peatlands (Raymond and Bauer 2001). Moreover, ultrahigh-resolution ion cyclotron resonance mass spectrometry can identify thousands of unique molecular formulae contained in a single water sample, offering an unparalleled window into the composition of natural organic matter (Koch et al. 2005). These data can be further leveraged to correlate relative abundances of each individual formulae with various environmental variables and gain more nuanced understanding of how certain OM pools vary and relate to one another (Behnke et al. 2021; Kurek et al. 2021). Overall, the application of such tools to characterize C in rivers can provide important insights into seasonal shifts in C sources as well as the mobilization of aged OC from erosion of long-term stocks in soils or peat reservoirs.

To assess the seasonality, composition, and fluxes of C from a unique endmember tributary to the Congo River, we examined the Ruki River for one hydrologic year from November 2019 to December 2020. We measured fortnightly concentrations of all major species of C borne by the river, including DOC, dissolved inorganic carbon (DIC), dissolved carbon dioxide ($p$$CO_2$), dissolved methane ($p$$CH_4$), and particulate organic carbon (POC). Using these concentrations and

their relationships with discharge, we modeled instantaneous daily fluxes and estimated the cumulative annual fluxes into the Congo mainstem. We additionally measured the carbon to nitrogen ratio (C : N) and stable and radiocarbon C isotopic ratios of dissolved and particulate organic matter (DOM and POM, respectively). These tracers provide information as the sources and cycling of C within the Ruki River, especially with respect to the identification of aged peat-derived OC. This study represents the first high-resolution exploration into the C biogeochemistry of a pristine African blackwater river. The results from this study can serve as a benchmark against which to assess the effects of future anticipated impacts such as deforestation or the drainage of peatlands.

Methods

Site description

The Ruki River is a large, left-bank, blackwater tributary that joins the Congo River at the city of Mbandaka, approximately 645 km upstream from Kinshasa-Brazzaville (Fig. 1A). The Ruki Basin spans 188,800 km^2, is relatively flat (min/max: 250/750 masl), and has an average elevation of ~ 400 m asl. It receives an average rainfall of ~ 2000 mm annually (derived from rainfall data detailed below). The land cover within the Ruki Basin is composed of mostly lowland evergreen broadleaf and swamp forests (together comprising 93.6% of the Basin area) and contains no urbanized areas and only minimal deforested and agriculturally converted areas (Fig. 1B). The lowland forests are dominated by stands of *Gilbertodendron dewevrei*, with other areas populated by semi-deciduous *Staudtia stipitata*, *Polyalthia suavaeoleus*, *Scorodophloeus zenkeri*, *Anonidium mannii*, and *Parinari glaberrimum*. The seasonally flooded swamp forests contain *Guibourtia demeusei*, *Mitragyna* spp., *Symphona globulifera*, *Entandrophragma palustre*, *Uapaca heudelotii*, *Sterculia subviolacea*, and *Alstonia congensis* while the permanently flood swamp forests contain monospecific stands of *Raffia* palm. The soils of the lowland evergreen and swamp forests are predominantly Ferralsols and Gleysols, respectively (Jones et al. 2013).

Owing to its low gradient, the Ruki River and its network of tributaries are slowly moving and placid. Like much of the interior Congo Basin, these river networks are the primary means of transportation and commerce among the inhabitants. The small upriver towns of Boende and Ingende are serviced by diesel boats, although there is one unmaintained road that traverses the basin.

Discharge and precipitation

Instantaneous river discharge (Q) was measured fortnightly during one hydrologic year (21 November 2019 to 30 November 2020; $n = 29$) at the narrowest section of the Ruki (~ 430 m width) at the Jardin Botanique d'Eala (0.0698 N, 18.3167E) using a Sontek RiverSurveyor M5 Acoustic Doppler Current Profiler mounted to a pirogue. Reported discharge values represent the average of four transects, the coefficient of variation of which never exceeded 1.3%. Daily water height measurements were measured at noon using a staff gauge installed at the Jardin Botanique d'Eala. A standard power function ($Q = a \times H^b$, Q = discharge, H = stage height, and a and b are constants) was fitted to the stage-discharge data and the resulting rating curve (see results below) was used to interpolate the fortnightly instantaneous measurements and generate a year-long discharge record for the Ruki.
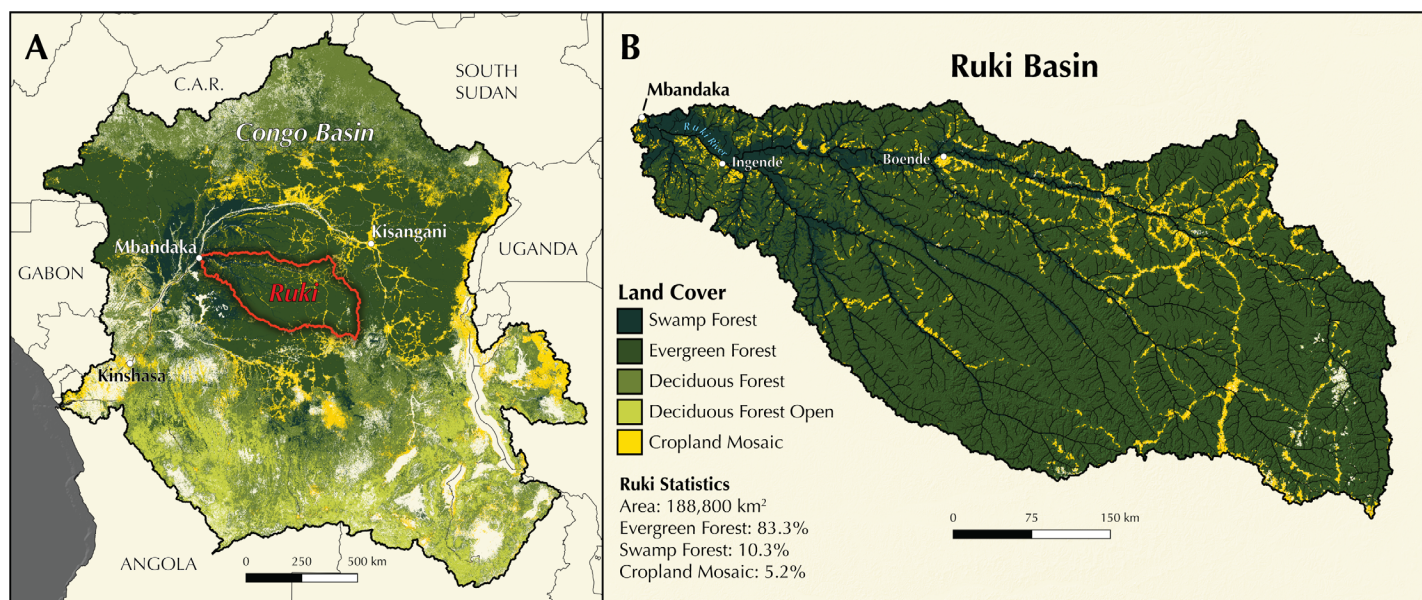

Fig. 1. Map of the Congo Basin (**A**) with the Ruki sub-basin highlighted in red. Detailed map of the Ruki Basin with sampling location at Mbandaka shown in panel (**B**). Land-cover data sourced from ESA CCI-LC 2021 data.

Monthly accumulated precipitation data (half-hourly multi-satellite precipitation estimate with gauge calibration - GPM_3IMERGHH_v06) for the study period was downloaded from the NASA Global Precipitation Measurement repository on the Giovanni hub (giovanni.gsfc.nasa.gov/) and clipped to the Ruki catchment area and averaged using QGIS raster tools.

Sample collection and processing

On the same days and at the same location that discharge was measured, river samples were collected from the center of the channel directly offshore from the Jardin Botanique d'Eala using a motorized pirogue. At each sampling event, water for dissolved constituents was pumped from a depth of 0.5 m through a pre-combusted (450°C, >5 h) 0.7 μm glass fiber filter (Whatman GF/F) using a peristaltic pump into opaque acid-leached HDPE bottles and four 20 mL pre-combusted (450°C, >5 h) glass vials. Using a weighted intake tube and the peristaltic pump, unfiltered water for particulate constituents was pumped from approximately two-thirds depth of the center of the channel (as determined by the ADCP measurement, section 1.3) into two prerinsed 10 L Nalgene bottles. DIC, carbon dioxide (CO_2) and methane (CH_4) were sampled by injecting 6 mL of bubble-free river water taken 0.5 m below the river surface with a syringe into six N_2 flushed, gas-tight exetainers (12 mL, Labco, UK). Prior to sampling and N_2 flushing, three of the exetainers were dosed with 10 μL of 12 M HCl (to shift the pH < 2 and convert all carbonate species into CO_2 for DIC analysis) and all six exetainers were treated with 5 μL of 50% $ZnCl_2^-$ (to suppress microbial activity). River water isotopes were sampled with 3 mL Exetainer vials filled to the brim using a syringe. Water pH was measured with a precalibrated portable pH meter (VWR pH 20) at a depth of 30 cm in the river.

In a clean room at the Woodwell Climate Research Center in Mbandaka, filtered samples DOC, DOM, and isotope analyses were acidified to a pH of 2 with 12 M HCl and stored in acid-leached HDPE bottles in a dark, cool place prior to transport to Zurich, Switzerland. Given the high DOC concentrations in the Ruki, samples were kept unfrozen to reduce the loss of DOC via solute exclusion and precipitation during ice formation (Fellman et al. 2008). Unfiltered water samples were agitated to re-suspend sediments and then filtered onto precombusted (450°C, >5 h) and preweighed 0.7 μm Whatmann GF/F filters. The amount of water passed through each filter was determined using a graduated cylinder and recorded. Filters were then sealed in plastic cases and frozen prior to transport. After transport to Zurich, the filters were thawed and dried at 60°C for 48 h.

Carbon, nitrogen, and water analyses

Concentrations of DOC and total dissolved nitrogen (TDN) were measured on the filtered water samples via high-temperature catalytic oxidation on a Shimadzu TOC-L total organic carbon analyzer equipped with a TNM-1 module using

established methodology (Drake et al. 2018*a*). For this study, we report DOM C : N ratios as DOC : TDN, since dissolved organic nitrogen was not derived for all samples but determined to consistently comprise an average of 90% of TDN in preliminary analyses. Thus, our reported C : N ratios are slightly lower than actual DOM C : N ratios but still reflective of relative shifts in OM sources. Stable ($\delta^{13}C$) and radiocarbon (^{14}C contents) compositions of OC were determined via isotope ratio mass spectrometry (0.1‰ precision) and accelerator mass spectrometry, respectively, at the Laboratory of Ion Beam Physics (LIP) using established procedures (Mcintyre et al. 2017). For DOC preparation, 150 mL of acidified DOC samples were concentrated using a freeze drier. Concentrated DOC samples (50–100 μg C) were converted to CO_2 using wet chemical oxidation. Sodium persulfate was then added to each of two 6 mL aliquots of the concentrated water in 12 mL gas-tight exetainer Labco vials. Prior to oxidation, inorganic CO_2 was removed by sparging the vials with He gas. The vials were then heated to 100°C for 1 h to convert the DOC to CO_2. The CO_2 from one exetainer was then analyzed for $\delta^{13}C$ on a Thermo Scientific Gas Bench II at ETH Zurich. We report $^{13}C/^{12}C$ in traditional "delta" notation as $\delta^{13}C = (^{13}R_{sample}/^{13}R_{VPDB} - 1) \times 1000‰$, where ^{13}R is the $^{13}C/^{12}C$ ratio, VPDB is the Vienna Pee Dee Belemnite reference standard, and "‰" indicates parts per thousand. The formed CO_2 in the headspace of the second aliquot was analyzed for ^{14}C activity using a mini carbon dating accelerator mass spectrometer (MICADAS) system equipped with a gas-accepting ion source at the LIP at ETH Zurich (Wacker et al. 2010). The samples have been corrected for constant contamination method (Haghipour et al. 2019) using processed blanks and standards (sucrose: Sigma, $\delta^{13}C = -12.4‰$, $F_m = 1.053 \pm 0.003$ and phthalic acid: Sigma, $\delta^{13}C = -33.6‰$, $F_m < 0.0025$). Measured $^{14}C/^{12}C$ ratios are reported as fraction modern ^{14}C activity (F_m, as described in Stuiver and Polach 1977). ^{14}C analyses were prioritized when there was only one aliquot of CO_2 derived from the freeze-dried DOC, hence only five samples were analyzed for ^{13}C-DOC.

Dissolved organic matter (DOM) in river samples was isolated for Fourier transform ion cyclotron resonance mass spectrometry (FT-ICR-MS) analysis via solid-phase extraction with 100 mg Bond Elut (Agilent Technologies) styrene-divinylbenzene copolymer (PPL) cartridges. Using a sample's DOC concentration, the volume of water used for extraction was adjusted to target 50 μg of C eluted with 1 mL of HPLC-grade methanol into a precombusted glass vial. The molecular composition of acidic species from PPL-extracted DOM was determined by negative-ion micro-electrospray ionization coupled to a 21 Tesla FT-ICR-MS at the National Magnetic Field Laboratory at Florida State University, USA (Smith et al. 2018; Hendrickson et al. 2015). Typical conditions for negative ion formation were: emitter voltage of − 2.4–2.9 kV, S-lens RF level at 45%, and a heated metal capillary temperature of 350°C with a 500 nL min^{-1} flow rate. Time-domain transients of 3.1 s were conditionally co-added

and acquired with the Predator data station, with 100 time-domain acquisitions averaged for all experiments, which were initiated by a TTL trigger from the commercial Thermo data station (Blakney et al. 2011). Mass spectra were phase-corrected and internally calibrated with 10–15 highly abundant homologous series that span the entire molecular weight distribution based on the "walking" calibration method (Xian et al. 2010; Savory et al. 2011). Peaks with signal magnitude greater than six times the baseline root-mean-square (rms) noise at m/z 500 were exported to peak lists and elemental compositions were assigned based on constraints published (Koch et al. 2007; Stubbins et al. 2010) on all signals $> 6\sigma$ root mean square baseline noise with PetroOrg© software (Corilo 2014). Molecular formulae with elemental combinations of $C_{4-50}H_{8-100}N_{0-4}O_{1-25}S_{0-2}$ and mass errors < 200 ppb were assigned. The modified aromaticity index (AI_{mod}) for each neutral elemental composition was calculated following the procedure of Koch and Dittmar (2006, 2016). Formulae were classified into compound classes by their elemental stoichiometries and AI_{mod} (Šantl-Temkiv et al. 2013). AI_{mod} values of 0.5 to 0.67 and > 0.67 were classified as aromatic and condensed aromatic structures, respectively. Further compound classes were defined as follows: condensed aromatic = $AI_{mod} > 0.67$, polyphenolic = $0.67 \geq AI_{mod} > 0.5$, unsaturated low oxygen = $AI_{mod} < 0.5$, H/C < 1.5, O/C < 0.5; unsaturated high oxygen = $AI_{mod} < 0.5$, H/C < 1.5, O/C > 0.5; aliphatics = H/C 1.5–2.0, O/C < 0.9, N = 0; and peptides = H/C 1.5–2.0, O/C < 0.9, N > 0.

Total suspended solids (TSS) concentrations were determined by dividing the weight difference between the pre-weighed filters and the dried filter after filtration by the amount of water filtered. POC and PON concentrations were determined by feeding the whole filter to an elemental analyzer (Automated Nitrogen Carbon Analyzer, SerCon; Crewe, UK).

Mole fractions of DIC, dissolved CO_2, and dissolved CH_4 were measured on equilibrated gas headspaces of the exetainers via gas chromatography (456-GC, Scion Instruments, UK) using a suite of standards that spanned the expected range of concentrations. Dissolved concentrations were calculated using headspace mole fractions and exetainer headspace/water volume ratios according to Henry's law.

All water samples were analyzed for δD and $δ^{18}O$ values using the high-temperature carbon reduction method by coupling a high-temperature elemental analyzer (TC/EA; Finnigan MAT, Bremen, Germany) to a Delta^{plus}XP isotope ratio mass spectrometer via a ConFlo III interface (Finnigan MAT; Werner et al. 1999). Post-run off-line calculations like offset-, memory effect- and drift corrections for assigning the final δD and $δ^{18}O$-values on the V-SMOW scale were performed according to Werner and Brand (2001). The long-term precision (3 yr) of the quality control lab standard water (Isolab 1, 4 replicates in a measurement sequence) for δD and $δ^{18}O$ was 0.57‰ and 0.22‰, respectively.

Flux estimates

Daily carbon fluxes (kg C d^{-1}) for all dissolved C species were modeled using instantaneous discharge measurements (m^3 s^{-1}) and concentration data input into the FORTRAN Load Estimator (LOADEST) program (Runkel et al. 2004). Daily fluxes were then summed for the study period to generate an annual flux estimate. For each C species, the LOADEST calibration equation was determined using the adjusted maximum likelihood estimate (AMLE) with the regression model number set to default (MODNO = 0), allowing the model to determine the best fitting regression using Akaike Information Criteria. The model output includes the standard error and the standard error of the prediction of the fluxes in addition to the r^2 of the AMLE, residuals, and the serial correlation of the residuals. These statistics allow for model validation and for confirmation that the residuals are normally distributed according to established protocols (Dornblaser and Striegl 2009).

CO_2 outgassing from the Ruki River water surface to the atmosphere was estimated from fortnightly pCO_2 concentrations. The flux to the atmosphere was calculated as $F = k_{CO2} \times \Delta pCO_2$, where k_{CO2} is the gas-transfer velocity of CO_2 and ΔpCO_2 is the difference between the partial pressure of CO_2 in the water and the atmosphere ($\Delta pCO_2 = CO_{2\text{-river}} - CO_{2\text{-atmosphere}}$). Monthly global average atmospheric pCO_2 concentrations for the study period were obtained from the National Oceanic and Atmospheric Administration's Global Monitoring Program (https://gml.noaa.gov/ccgg/trends/gl_data.html). A commonly used literature-derived standardized k_{600} value of 4.13 m d^{-1} for rivers > 100 m in width (Mann et al. 2014; Borges et al. 2015) was converted to a gas- and temperature-specific gas transfer velocity (k_{CO2}) using temperature-dependent Schmidt numbers for CO_2 (Raymond et al. 2012). pCO_2 concentrations measured during midday when in-stream photosynthesis is at its potential maximum and daily pCO_2 concentrations are at their potential minimum have the potential to underestimate daily average concentration (Gómez-Gener et al. 2021), however, previous work in Congo blackwater systems has shown that diel variations in pCO_2 are undetectable because phytoplankton primary production is light limited from high DOC concentrations (Borges et al. 2019, Descy et al. 2017).

Although the direct outgassing of greenhouse gasses from river surfaces to the atmosphere (i.e., vertical fluxes) has become increasingly recognized as an important and often dominant flux relative to lateral export, accurate quantification at the basin scale is still hindered by high spatio-temporal variability and the lack of spatially representative measurements. As a result, we only present local instantaneous fluxes from the water surface and refrain from offering a basin-wide estimate due to the inaccuracy of such estimates upscaled from a single location.

Statistical analyses

To test the shape of the concentration–discharge relationships, power law equations were fit to the data using least

squares regressions with the Prism Graphpad statistical software. For all regressions, 95% confidence intervals were calculated. Concentration-discharge data were fit with the power law equation:

$$C = a \times Q^b$$

where C is the solute concentration, Q is the water discharge, and a and b are fitted constants. The b exponent relates to the influence of mobilization (positive values), dilution (negative values), or chemostasis (values near zero; Godsey et al. 2009). The power law equation has supplanted linear regression as the preferred model for concentration-discharge relationships given the ability to evaluate C–Q patterns quantitatively with the b-exponent metric (Musolff et al. 2015; Rose et al. 2018).

FT-ICR MS data analysis for compound class statistics, heteroatomic content, and Spearman's rank correlations were performed with the "fouriertransform" Python package (Hemingway 2017).

Results and discussion

Ruki River hydrology

The average width of the Ruki at the study site was 490 m, the average velocity was 0.80 m s^{-1}, and the average depth was 9.5 m. Measured Ruki River water discharge ($n = 29$) ranged from 2348 to 5515 m^3 s^{-1} and averaged 3778 m^3 s^{-1} for the study period (Table 1). Daily stage height ranged from 0.47 to 3.51 m for the study period, with measured discharges spanning stage heights from 0.55 to 3.44 m (95% of the total range). Measured discharge related well to stage height when modeled with a power function ($r^2 = 0.85$, Supporting Information Fig. S1), likely due to slight hysteresis due to flood conditions near the confluence of Ruki and Congo Rivers. As a result, interpolated and modeled discharge values varied slightly from measured values and tended to be slightly lower during peak and low flows and slightly higher during moderate flows.

Total annual discharge for the Ruki was 115 km^3 yr^{-1}, which represents 8.6% of the average annual water flux of the Congo River at Kinshasa-Brazzaville (1336 km^3 yr^{-1}; Spencer et al. 2016). Like the Congo, the Ruki exhibited a bi-modal hydrograph with a dominant peak in December and a smaller second peak in June (Fig. 2). Intra-annual variability of the Ruki (measured daily max Q/min Q) was 2.35, slightly higher than the Congo average for 1977–2006 (1.94; Spencer et al. 2012). This relatively low seasonal variability in discharge arises due to the regular and high rainfall (1800–2200 mm) in the Central Basin, which dampens extremes in flow (Maurice 1947; Runge 2008).

Indeed, satellite-derived monthly average rainfall on the Ruki Basin area for the study period ranged from 98 to 239 mm, with an average of 162 mm. The total average rainfall for the study period was 1960 mm, which lies in the middle of the range for Central Congo. All values of monthly specific discharge (Q/drainage area) plotted against the corresponding monthly precipitation fell below the 1 : 1 line (Fig. 3), indicating high evapotranspiration rates in the watershed. Over the study period, the Ruki River discharged 31% the amount of water it received as rainfall over the Basin. Peak discharge (~ 75 mm) lagged approximately two and a half months behind peak rainfall (~ 230 mm), providing an average travel time for water in the Basin.

Stable isotopic values (δD and δ^{18}O) of Ruki River water ranged from -28.2 to $-0.5‰$ and -5.1 to $-2.1‰$, respectively (Table 1). Water isotopic ratios exhibited a strong seasonality (Fig. 2) and varied inversely with water discharge (Supporting Information Fig. S2). The depletion of δD and δ^{18}O during high flows corresponds to both the higher inputs of precipitation relative to baseflow and to the lower isotopic signature of precipitation during the wet season (basin-integrated average δD of rainfall is $-17.0‰$ for October compared to 15.7‰ for July; Terzer-Wassmuth et al. 2021).

Carbon concentration dynamics

DOC concentrations ranged from 12.7 to 30.1 mg L^{-1} and averaged 21.3 mg L^{-1} for the study period (Table 1). These concentrations are much higher than those observed in the Congo River (7.8–11.8 mg L^{-1}; Spencer et al. 2016) and other large tropical blackwater rivers such as the Rio Negro (7.1–10.8 mg L^{-1}; Richey et al. 1990; Pérez et al. 2011; Gonsior et al. 2016), Epulu River (5.2–9.0 mg L^{-1}; Spencer et al. 2010), or Caroní River (5.87 mg L^{-1}; Paolini et al. 1987). DOC concentrations exhibited a strong positive correlation with discharge, with a positive b-value (0.69) in the fitted power relationship indicating a mobilization or flushing response (Fig. 4A). No discernable hysteresis was observed in the DOC-discharge relationship, indicating a consistent supply of DOC sources available for mobilization throughout the year.

TSS and POC ranged from 0.68 to 6.89 and 0.39 to 1.61 mg L^{-1} and averaged 3.68 and 0.88 mg L^{-1}, respectively (Table 1). These TSS concentrations are much lower than those observed in the Congo mainstem (15.5–27.2 mg L^{-1}; Spencer et al. 2016) and large rivers globally (7.0–26,900 mg L^{-1}; Meybeck and Ragu 1997), while the POC concentrations are only slightly lower than in the Congo River (1.01–1.97 mg L^{-1}; Spencer et al. 2016). Compared to the Rio Negro, Ruki TSS concentrations are generally lower while POC concentrations are similar (Negro TSS: 3.7–11 mg L^{-1} and POC: 0.27–1.1 mg L^{-1}; Moreira-Turcq et al. 2003). The relative proportion of POC to TSS (%POC) in the Ruki was high, averaging 28% and generally exceeding the OC content of sediments within other tropical rivers (Fig. 5). The Ruki thus represents an end-member along the chemical weathering (low TSS and high POC) to mechanical erosion (high TSS and low POC) continuum of rivers, exemplifying a tropical basin with minimal mechanical erosion and very low sediment mobilization (Seyler et al. 2005). Indeed, TSS and POC

Table 1. Water discharge (Q), water deuterium (δD) and oxygen ($\delta^{18}O$) isotopes, carbon and nitrogen concentrations, carbon isotopic ratios, C : N ratios, and TSS for the Ruki River over the study period.

| Date	Q	δD	$\delta^{18}O$	DOC Conc.	DOC $\delta^{13}C$	DOC F_m	TDN	DOM C : N	TSS	POC Conc.	POC $\delta^{13}C$	POC F_m	PN	POM C : N	DIC	pCO_2	pCH_4
	(m³ s⁻¹)	(‰)	(‰)	(mg C L⁻¹)	(‰)		(mg N L⁻¹)	(molar)	(mg L⁻¹)	(mg C L⁻¹)	(‰)		(mg N L⁻¹)	(molar)	(mg C L⁻¹)	(ppm)	(ppm)
21.11.19	4'690	−28.2	−5.1	30.1	−30.7	1.07	0.91	38.4	1.10	0.45	−32.0	0.97	0.044	11.8	4.8	8301	413
25.11.19	4'969	−22.3	−4.6	26.5	−29.7	1.06	0.88	35.3	1.33	0.44	−33.3	0.98	0.039	13.2	4.9	8198	237
02.12.19	5'340	−19.0	−4.3	27.8		1.07	0.90	36.1	0.68	0.39		0.97	0.038	12.1	5.2	8476	389
16.12.19	5'515	−17.5	−4.1	28.2	−30.0		0.88	37.2	3.68	0.43	−33.1	0.97	0.045	11.2	5.2	8190	471
30.12.19	5'320	−18.7	−4.3	25.8		1.05	0.82	36.8	3.21	0.49	−32.9	0.98	0.049	11.7	5.2	8047	230
13.01.20	5'192	−12.8	−3.6	22.9		1.06	0.77	34.8	1.54	0.53	−33.4	0.97	0.047	13.0	5.4	7485	289
27.01.20	5'267	−5.4	−2.7	21.8	−29.9	0.98	0.79	32.2	1.76	0.66	−37.2	0.99	0.086	8.9	5.8	7459	517
10.02.20	4'299	−5.1	−2.5	22.4	−31.0	0.86	0.68	38.2	4.38	0.76	−31.8	0.94	0.068	13.0	6.3	7381	
24.02.20	3'054	−3.5	−2.7	16.4		1.06	0.71	27.0	4.98	0.96	−32.4	0.88	0.084	13.3	4.9	4925	163
09.03.20	2'637	−2.4	−2.4	15.2		1.07	0.57	31.3	6.89	1.33	−30.9	0.96	0.107	14.6	4.5	4648	133
23.03.20	3'571	−5.0	−2.7	18.2		1.06	0.71	30.0	3.78	0.73	−30.7	0.96	0.062	13.8	5.5	6584	248
07.04.20	3'492	−10.0	−3.3	19.5		1.05	0.69	32.9	4.69	0.81	−31.1	0.95	0.079	12.0	5.6	5912	263
20.04.20	3'086	−8.8	−3.1	14.7		1.05	0.55	30.9	4.57	0.79	−30.6	0.96	0.066	14.0	4.8	4198	182
04.05.20	3'190	−10.0	−3.2	16.6		1.05	0.63	30.8	5.66	0.88	−31.0	0.98	0.078	13.1	5.1	5453	281
18.05.20	3'223	−14.7	−3.8	19.0		1.06	0.65	33.9	3.15	0.54	−30.9	0.96	0.048	13.2	6.3	5817	175
01.06.20	3'591	−12.5	−3.6	22.4		1.06	0.77	34.0	3.22	0.70	−32.3	0.95	0.058	14.1	6.8	6240	267
15.06.20	3'298	−5.7	−2.8	19.1		1.05	0.62	35.8	4.67	1.04	−31.1	0.94	0.068	17.9	5.7	5734	198
29.06.20	2'514	−2.8	−2.3	17.7		1.05	0.72	28.8	4.70	1.02	−31.8	0.97	0.074	16.1	5.5	4974	308
14.07.20	2'379	−1.2	−2.2	16.0			0.70	26.5	3.57	1.23	−30.8	0.93	0.075	19.2	4.8	3395	255
27.07.20	2'988	−1.5	−2.2	20.8		1.05	0.74	32.7	3.81	1.26	−31.4	0.94	0.075	19.6	5.8	4989	156
10.08.20	2'594	−1.1	−2.1	19.8		1.06	0.69	33.7	4.99	1.06		0.94	0.077	16.1	5.4	4443	117
25.08.20	2'348	−0.5	−2.1	14.8		1.05	0.66	26.1	5.77	1.61	−31.2	0.92	0.096	19.6	5.4	3467	132
07.09.20	2'483	−3.6	−2.4	12.7		1.03	0.58	25.4	5.71	1.27	−30.1	0.93	0.098	15.0	4.8	3069	117
28.09.20	3'823	−9.3	−3.4	25.3		1.06	0.87	34.0	4.49	1.11	−30.8	0.94	0.075	17.3	7.7	7946	293
05.10.20	3'810	−11.7	−3.5	24.2		1.03	0.77	36.5	2.72	1.03	−30.5	0.93	0.070	17.2	7.0	8264	185
19.10.20	3'821	−14.2	−3.9	22.5		1.07	0.71	37.0	2.11	1.25	−37.2	0.94	0.104	14.0	7.0	7111	219
02.11.20	3'879	−17.3	−4.3	23.7		1.06	0.73	38.1	2.03	1.05	−31.1	0.94	0.110	11.1	7.1	7185	194
16.11.20	4'456	−19.0	−4.5	26.2		1.07	0.81	37.9							7.0	7643	343
30.11.20	4'728	−16.0	−4.1	28.7		1.06	0.86	39.0							7.4	9088	239
Min	2'348	−28.2	−5.1	12.7	−31.0	0.86	0.55	25.4	0.68	0.39	−37.2	0.88	0.04	8.9	4.5	3069	117
Max	5'515	−0.5	−2.1	30.1	−29.7	1.07	0.91	39.0	6.89	1.61	−30.1	0.99	0.11	19.6	7.7	9088	517
Average	3'778	−10.3	−3.3	21.3	−30.3	1.05	0.74	33.5	3.68	0.88	−32.0	0.95	0.07	14.3	5.7	6366	251
C.V. (%)	27	71.3	26.5	22.4	1.80	3.86	13.65	11.9	43.81	37.42	5.7	2.42	29.28	19.3	15.9	27	41
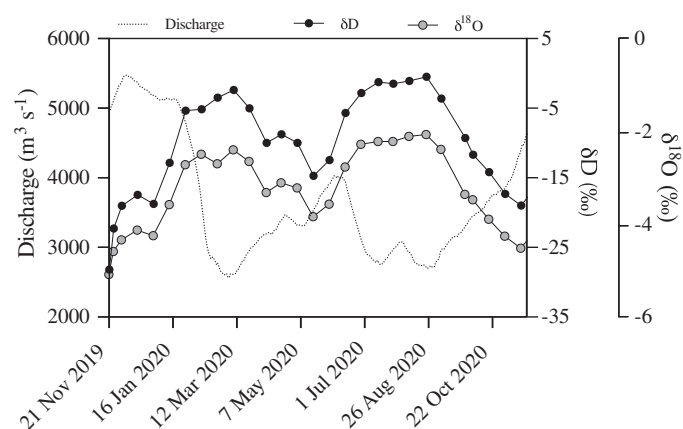
Fig. 2. Discharge (dotted line) and water isotopes (δD–black circles; δ^{18}O–gray circles) time-series for the Ruki River at Mbandaka, Democratic Republic of Congo. Note the separate axes and ranges for δD and δ^{18}O on the right.

concentrations were both negatively correlated with discharge (*b*-values of -1.03 and -0.85, respectively), indicating a dilution response to increased flow (Fig. 4B,C).

DIC concentrations ranged from 4.5 to 7.7 mg L^{-1} and averaged 5.7 mg L^{-1} for the study period (Table 1). This range of DIC concentrations is higher than average values for the Congo River (3.1 mg L^{-1}; Wang et al. 2013) and an order of magnitude higher than values for the Rio Negro (0.4 ± 0.2; de Fátima et al. 2013). However, like the Congo River, Ruki DIC did not exhibit a significant relationship with discharge; DIC increased slightly with moderate discharge but decreased again at high flows (Fig. 4D). This pattern could be due to a

Fig. 3. Ruki River specific discharge vs. average rainfall for the basin area colored by month of the year.

decrease in pH with discharge driven by the increasing concentration of DOC and associated organic acids that have a titrating effect on DIC (Fig. 4D; Wang et al. 2013). The potential effect of DOC on the carbonate equilibrium system is also supported by the strong negative relationship between DOC and pH ($r^2 = 0.61$; Supporting Information Fig. S3). At low pH, bicarbonate ions are protonated and the DIC system shifts toward carbonic acid, which equilibrates with pCO$_2$. Ruki pCO$_2$ concentrations ranged from 3069 to 9088 ppm by volume (1.34–3.95 mg C L^{-1}) and averaged 6366 ppm (2.77 mg L^{-1}; Table 1). These values compare well to two CO$_2$ concentrations, 8686 and 6326 ppm, measured previously on the Ruki during the larger (December) and smaller (June) discharge peaks, respectively (Borges et al. 2019). Ruki pCO$_2$ concentrations from this study are higher than those measured in the Congo River at Kinshasa-Brazzaville (2018–6853 ppm; Wang et al. 2013) and the Rio Negro (1724–4720 ppm; de Fátima et al. 2013) but within the range for tropical rivers of the Congo Basin (2000–16,000 ppm; Mann et al. 2014; Borges et al. 2015) and close to the average concentration reported in African rivers (6415 ppm; Borges et al. 2015). Like DOC, Ruki pCO$_2$ concentrations exhibited a strong positive relationship with discharge (Fig. 4E). Such a relationship could indicate the increased mobilization of soil or wetland-derived CO$_2$ to the Ruki with higher flows. It also could arise from the increase in DOC that occurs with discharge, since higher DOC concentrations might fuel higher rates of heterotrophic respiration. However, given the observed pattern in DIC, this strong correlation with discharge might further indicate that it was the DOC titration effect on DIC that increased pCO$_2$ concentrations at high discharge. Indeed, the coefficient of variation (CV) for DIC was only 16% while pCO$_2$ had a CV of 27%, slightly higher than that of DOC (21%). These results suggest that pCO$_2$ would most likely have shown less seasonal variation if DOC concentrations had remained static.

pCH$_4$ concentrations ranged from 117 to 517 ppm, with an average of 251 ppm for the study period (Table 1). These concentrations compare well and envelope the two previous CH$_4$ concentrations, 346 and 254 ppm, measured during the larger (December) and smaller (June) discharge peaks, respectively (Borges et al. 2019). The seasonal range of pCH$_4$ concentrations in the Ruki River from this study corresponds well with the median ranges of pCH$_4$ measured within large and small rivers of the Congo Basin (~ 100–550 ppm; Borges et al. 2015). pCH$_4$ showed a moderate positive relationship with discharge ($R^2 = 0.49$) and suggests that the fluvial network becomes more hydrologically connected with wetlands at high flow.

Overall, C concentrations in the Ruki River were strongly controlled by hydrology. High flows mobilized plentifully available DOC from the watershed and allow for drainage of CH$_4$-rich wetlands. In turn, organic acids from these terrestrial or wetland inputs likely exerted a titration effect on DIC, shifting the carbonate equilibrium toward carbonic acid and
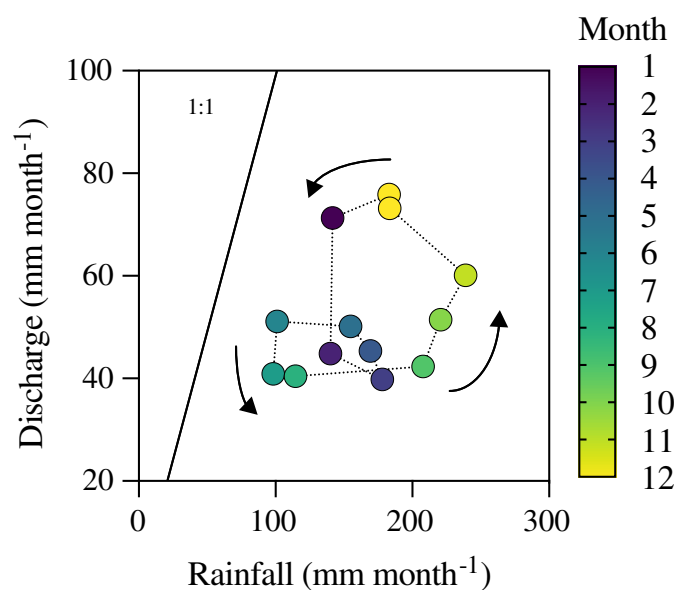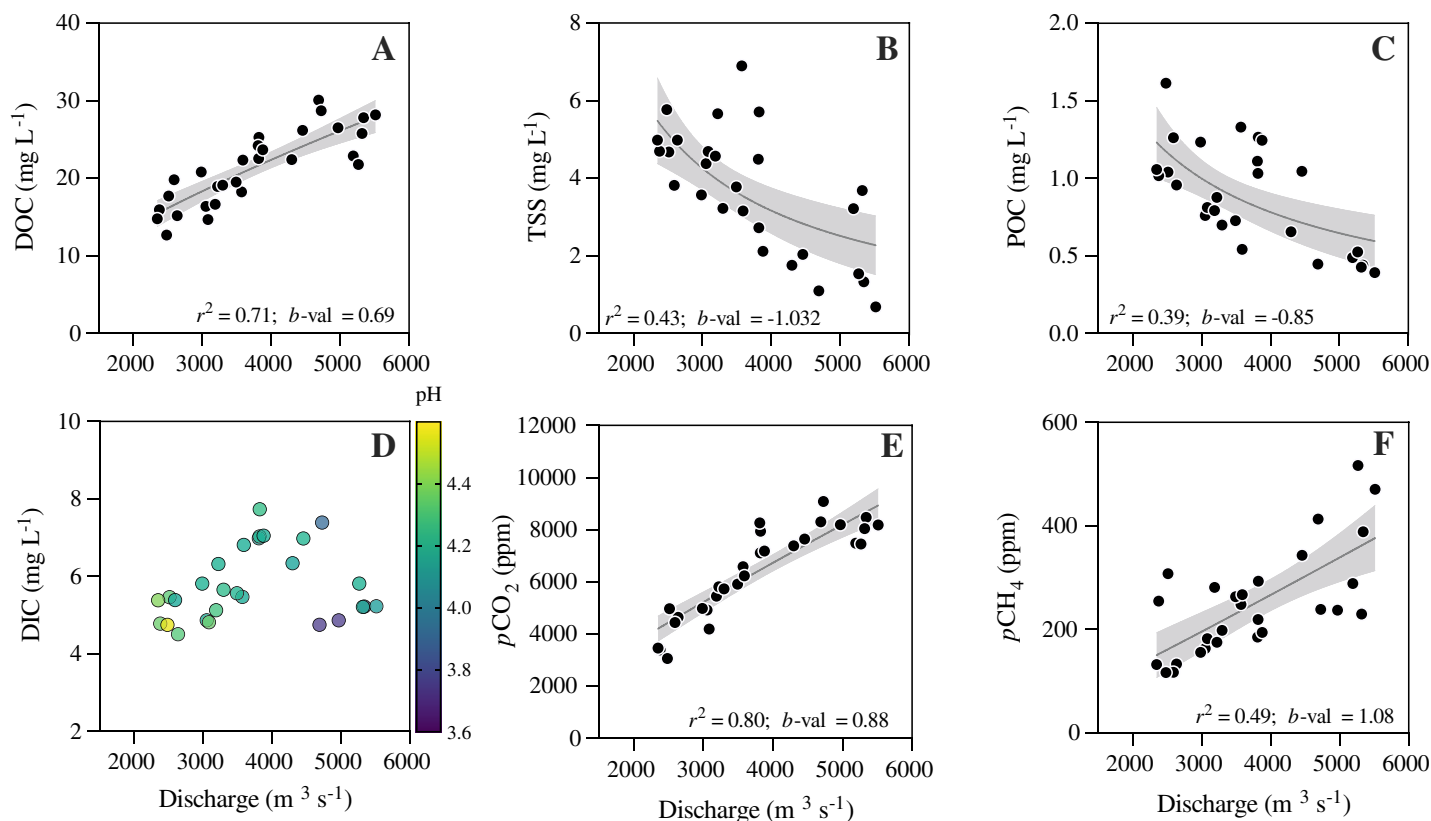
Fig. 4. DOC (**A**), total suspended sediment (**B**), POC (**C**), DIC (**D**), pCO$_2$ (**E**), and pCH$_4$ (**F**) correlated with discharge. Power regressions (gray line) are shown with 95% confidence intervals (light gray bands).

strongly increasing the concentration of pCO$_2$. Moreover, these higher DOC inputs may have also fueled more CO$_2$ production at high discharge. In contrast to the generally high concentrations and enrichment of dissolved C with discharge,

POC exhibited a dilution response and indicated the predominance of chemical weathering over physical erosion in this low-lying tropical basin.
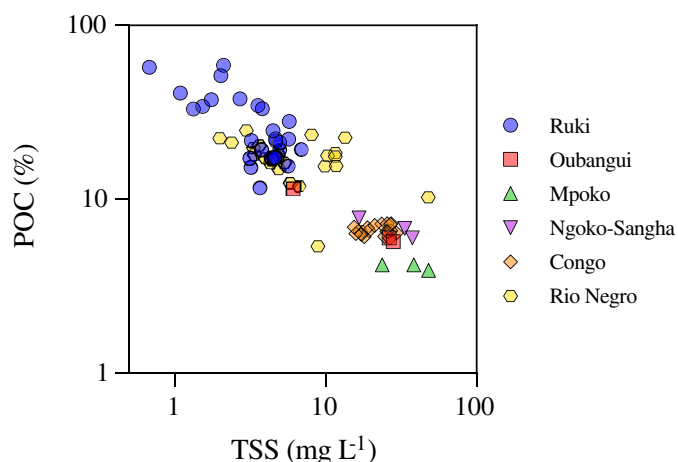

Fig. 5. Proportion of OC in total suspended sediments as a function of total suspended sediment concentration for the Ruki (this study) and other tropical rivers. Data sourced from (Moreira-Turcq et al. 2003; Coynel et al. 2005; Spencer et al. 2016).
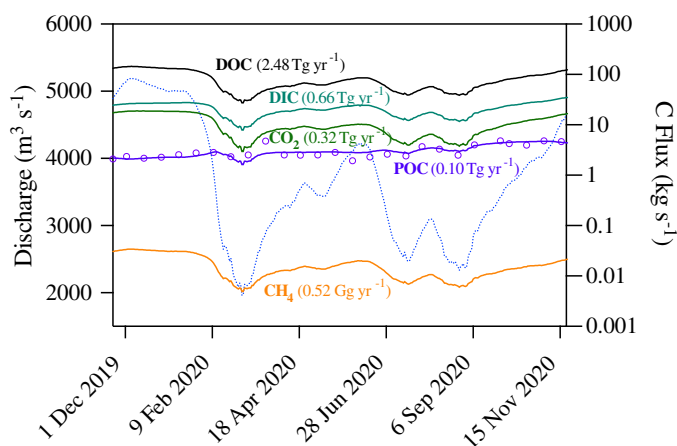

Fig. 6. LOADEST modeled instantaneous downstream fluxes of DOC (black), DIC (light blue), CO$_2$ (green), POC (purple), and CH$_4$ (orange). Calculated POC fluxes (discharge × concentration) are shown as purple circles. Total annual flux of each C species is shown in parentheses. Discharge is shown as a dotted blue line.

Fluxes of carbon

Given the predominantly positive relationships between dissolved C concentrations and discharge, the resultant modeled fluxes tended to track discharge (Fig. 6). Thus, periods of high flow are disproportionately important periods for the export of dissolved C in the Ruki Basin due to high concentrations of C species concurrent with elevated discharge (Figs. 4 and 6 and Table 1). The annual total flux of DOC was 2.48 Tg C yr^{-1}, which equates to a yield of 13 g m^{-2} yr^{-1} (Table 2). This high DOC yield highlights the Ruki as one of the most efficient exporters of DOC globally, registering at 1.5 × the yield of the Rio Negro (8.7 g m^{-2} yr^{-1}; Seyler et al. 2005), 1.5 × the Canoni River (9 g m^{-2} yr^{-1}; Paolini et al. 1987), 3.9 × the Congo (3.4 g m^{-2} yr^{-1}; Spencer et al. 2016), and almost 20 × the Mississippi River (0.7 g m^{-2} yr^{-1}; Raymond and Spencer 2015). Moreover, the annual flux of DOC from the Ruki represents ∼ 20% of the Congo Basin's total flux (12.48 Tg; Spencer et al. 2016), despite only comprising 5% of the Congo Basin by area. Similarly, DIC and lateral CO_2 fluxes (0.66 and 0.32 Tg, respectively; Table 2) comprised 19% and 16% of the Congo's annual DIC and lateral CO_2 fluxes (3.46 and 2.0 Tg; Wang et al. 2013), once again highlighting the C saturation of the Ruki relative to the Congo River. The downstream flux of CH_4 was considerably lower than CO_2, with only 0.52 Gg of C exported per year as CH_4 (Table 2).

Given the inverse relationship between POC concentration and discharge (Fig. 4C), POC fluxes were relatively invariant across the study year despite the strong fluctuations in discharge (Fig. 6). POC fluxes amounted to only 0.10 Tg yr^{-1} and represented 5% of the Congo's annual POC flux (1.96 Tg yr^{-1}; Table 2). In summary, the total downstream C flux from the Ruki River for the study period was 3.25 Tg yr^{-1}, of which DOC, DIC, and POC comprised 76.6%, 20.3%, and 3.1%, respectively. These results highlight the dominance of dissolved C species in the Ruki, a typical characteristic of placid, low-elevation, blackwater rivers.

Instantaneous outgassing CO_2 fluxes from our study site on the Ruki ranged from 5.5 to 18.1 g C m^{-2} d^{-1} and averaged 12.4 g C m^{-2} d^{-1}. Because CO_2 concentrations increased sharply with discharge, the CO_2 outgassing fluxes also exhibited a strong positive relationship with discharge

(Supporting Information Fig. S4). The seasonal range of CO_2 outgassing fluxes for the Ruki were similar to average values of rivers throughout the Congo Basin (13.8–18.2 g C m^{-2} d^{-1}; Borges et al. 2015) and forest-dominated rivers (> 100 m in width) in the Republic of Congo (10.3 g C m^{-2} d^{-1}; Mann et al. 2014). Outgassing fluxes were higher in the Ruki compared to the Oubangui River (0.3–0.6 g m^{-2} d^{-1}; Bouillon et al. 2012), a large right-bank tributary to the Congo that drains predominantly wooded savannah. This difference is likely the result of the Ruki's much higher pCO_2 concentrations that arise from a combination of higher inputs of both soil-derived pCO_2 and organic acidity from inundated lowland forests and greater overall mineralization within the river driven by the high DOC concentrations.

Collectively, these flux results demonstrate the overall importance of the Ruki River as a major transporter of dissolved C in-and-of itself and relative to its areal extent within the Congo Basin. Furthermore, these results highlight the dominant control of hydrology in dissolved C transport and how high flows may indirectly enhance the physical (mobilization), chemical (acid titration of carbonate system), and biological (heterotrophic respiration) transfer of CO_2 to the atmosphere in the Ruki Basin. Future work might endeavor to better partition the relationship between seasonal organic acid inputs and CO_2 outgassing in blackwater and other DOC-rich rivers.

Isotopic and molecular composition of DOC, POC, and DOM

Stable carbon isotopic ratios of DOC and POC ranged from − 31.0 to − 29.7‰ and − 36.3 to − 28.5‰, respectively (Table 1; Fig. 7A). In general, such depleted $\delta^{13}C$ values indicate that OC in the Ruki River is ubiquitously sourced from biogenic C fixed via the C3 photosynthetic pathway. Given the dominance of C3 plants in the Basin, such a mono-dominant source of OC in the river is expected. Indeed, the $\delta^{13}C$-POC values measured in the Ruki River were generally more depleted than average values for the Congo (− 28 to − 26.4‰; Spencer et al. 2016) and Oubangui (− 30.6 to − 25.8‰; Bouillon et al. 2012), both rivers that contain large proportions of savannah woodlands and C4 vegetation. Despite the dominance of a C3 source, Ruki $\delta^{13}C$-POC ratios

Table 2. Annual fluxes and yields of carbon by species for the Ruki and Congo Rivers. Congo River OC and DIC/CO_2 data sourced from Spencer et al. 2016 and Wang et al. 2013, respectively.

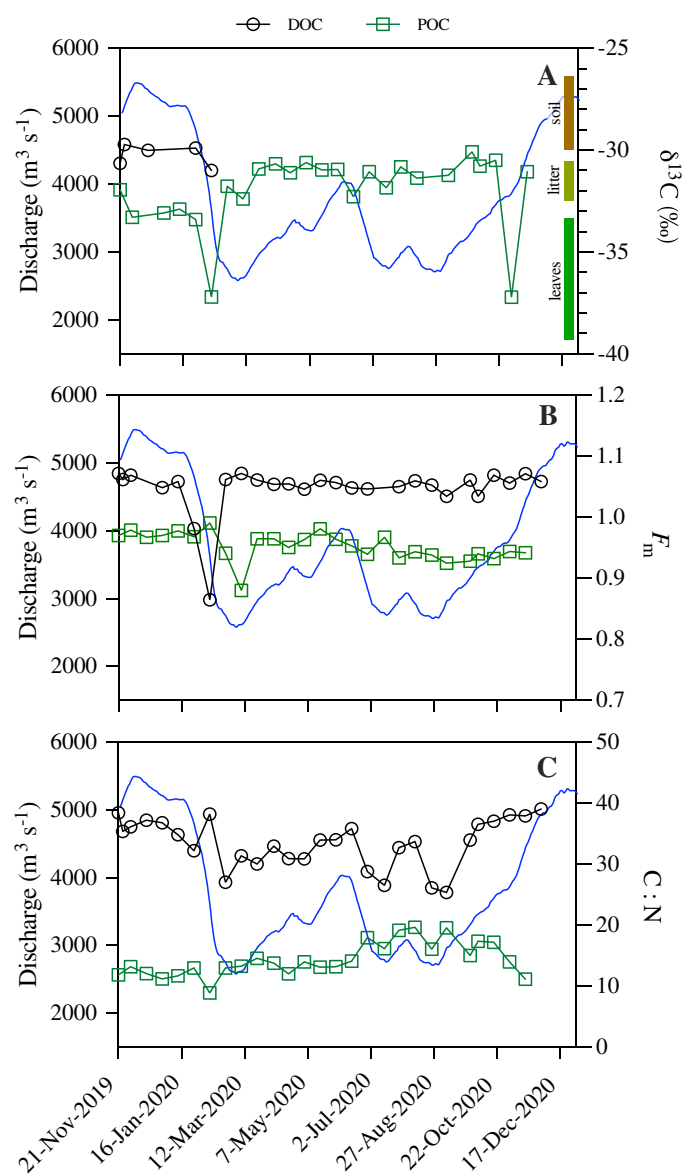|	Ruki		Congo		Ruki : Congo	
	Flux (Tg yr^{-1})	Yield (g m^{-2} yr^{-1})	Flux (Tg yr^{-1})	Yield (g m^{-2} yr^{-1})	Flux (%)	Yield (×)
DOC	2.48	13.14	12.48	3.40	20	3.9
POC	0.10	0.52	1.96	0.53	5	1.0
DIC	0.66	3.50	3.46	0.94	19	3.7
$CO_{2\text{-lateral}}$	0.32	1.69	2.00	0.55	16	3.1
CH_4	5.17×10^{-4}	2.74×10^{-3}				

Fig. 7. Timeseries of stable carbon isotopic ratios ($\delta^{13}C$) (**A**), the fraction of OC that is modern in age (F_m) (**B**), and C : N ratios (**C**) of DOC (black circles) and POC (green squares) measured in the Ruki River. Discharge is plotted for each dataset in blue. Stable carbon isotopic ranges for Congo lowland and swamp forest soil, litter, and plant leaves are shown on the right side of plot A (isotope data sourced from Baumgartner et al. (2020) and previously unpublished swamp forest data, see Supplemental Data S1). Note that the C : N ratio of DOM was calculated as DOC : TDN (see methods for explanation).

become hydrologically connected to the river system during peak flows.

The radiocarbon contents of DOC in the Ruki River were predominantly modern ($F_m > 1.00$; Table 1; Fig. 7B), indicating that DOC is sourced from recently photosynthesized vegetation or litter. Similarly, POC radiocarbon values were mostly modern (Fig. 7B), with values indicating slightly older C ages than DOC (Avg. F_m of 0.95; Table 1). The observed pattern of older POC ages relative to DOC is consistent with OC ages in African freshwaters and rivers globally (Marwick et al. 2015). The Ruki's average ^{14}C-POC content ($F_m = 0.95$) was similar to the averages from African rivers ($F_m = 0.97$; Marwick et al. 2015).

Interestingly, two timepoints on the falling limb of the most prominent discharge peak exhibited shifts toward older ^{14}C contents for both DOC and POC, with F_m values of 0.98 and 0.86 for DOC and 0.94 and 0.88 for POC (Fig. 7B). For DOC, the timing of these older values on the falling limb coincides with the highest proportion of subsurface flow of a typical flood hydrograph (Hursh and Brater 1941). This transition from surface runoff to subsurface flow on the falling limb is also evidenced by the shift to more enriched water isotopic ratios during this period (Fig. 2). If the DOC and H_2O isotopic ratios are the result of aged DOC arriving within subsurface water, they may indicate the presence of aged soil OC or even peat-derived OC in the bulk DOC pool. The dip in POC age occurred 1 month later than DOC (Fig. 7B), coinciding with minimum discharge and thus highest TSS/POC concentrations (Fig. 4). If the similarity in age between the oldest DOC and POC values (F_m of 0.88 and 0.86, respectively) reflects a common source, then the offset between the oldest DOC and POC values is likely explained by the divergent mobilization responses observed between the dissolved and particulate phases (Fig. 4).

The slight increase in C : N ratio (Fig. 7C) of DOM along with the sharp decrease in $\delta^{13}C$-POC at this time (Fig. 7A) may suggest a unique source of OC material mixing into the Ruki during the falling limb. Given that the oldest DOC value exhibited a high C : N ratio of DOM (~ 38) and a more depleted $\delta^{13}C$ signature (-31.0‰) relative to the range of values (C : N = 25.4–39.0, $\delta^{13}C = -30.7$ to -29.7‰), it is likely that this old OC was sourced from non-degraded peat rather than aged soil OC, which would have a lower C : N ratio as a result of microbial processing and necromass (Boström et al. 2007). Previous studies have also inferred the mobilization of peat-derived OC from the presence of aged material in water draining deeper subsurface flows, however, these studies took place in disturbed rather than pristine peatlands (Moore et al. 2013; Cook et al. 2018). Given the isolated nature of the aged signature in our dataset, the presence of peat OC in the Ruki River during the falling limb needs to be corroborated with additional high-resolution sampling. Nevertheless, the presence of aged material in the Ruki indicates some amount of mobilization of old C stores within the

exhibited slight seasonality, becoming slightly more enriched as discharge increased during the rising limbs before shifting to a more depleted signature at peak flows (Fig. 7A). This pattern suggests that the stock of more processed material in the Ruki Basin, presumably sourced from litter or top soils, is exhausted and replaced by either fresher, less degraded material or autochthonous biomass sourced from lakes that

Basin, which is an interesting finding given the generally low level of human impact on an areal basis.

The composition of DOM determined via FT-ICR MS revealed that the proportions of broad compound classes were stable throughout the study period (Supporting Information Fig. S5). This finding indicates a high level of seasonal homogeneity and consistent source of DOM to the River. Ruki DOM was characterized by high proportions of unsaturated phenolic and polyphenolic compounds, which is typical of DOM in natural waters sourced predominantly from terrestrial vegetation (Wagner et al. 2015). Compared to the Congo River, the

Ruki had higher oxygen-rich (O/C > 0.5) unsaturated phenolics (55.75% vs 38.4%), lower oxygen-poor (O/C < 0.5) unsaturated phenolics (21.8% vs. 38.4%), lower condensed aromatics (3.2% vs. 4.9%), and lower aliphatics (1.2% vs 3.7%; Kurek et al. 2022). The Ruki also exhibited higher relative abundances of CHON and CHOS (20.1% and 3.1%, respectively) than the Congo (13.9% and 2.4%, respectively; Kurek et al. 2022). These results suggest that DOM in the Ruki is more processed, oxidized, and heteroatomic, indicating higher relative inputs of degraded OM derived from decomposed litter and N- and S-rich soils. Meanwhile the Congo contains
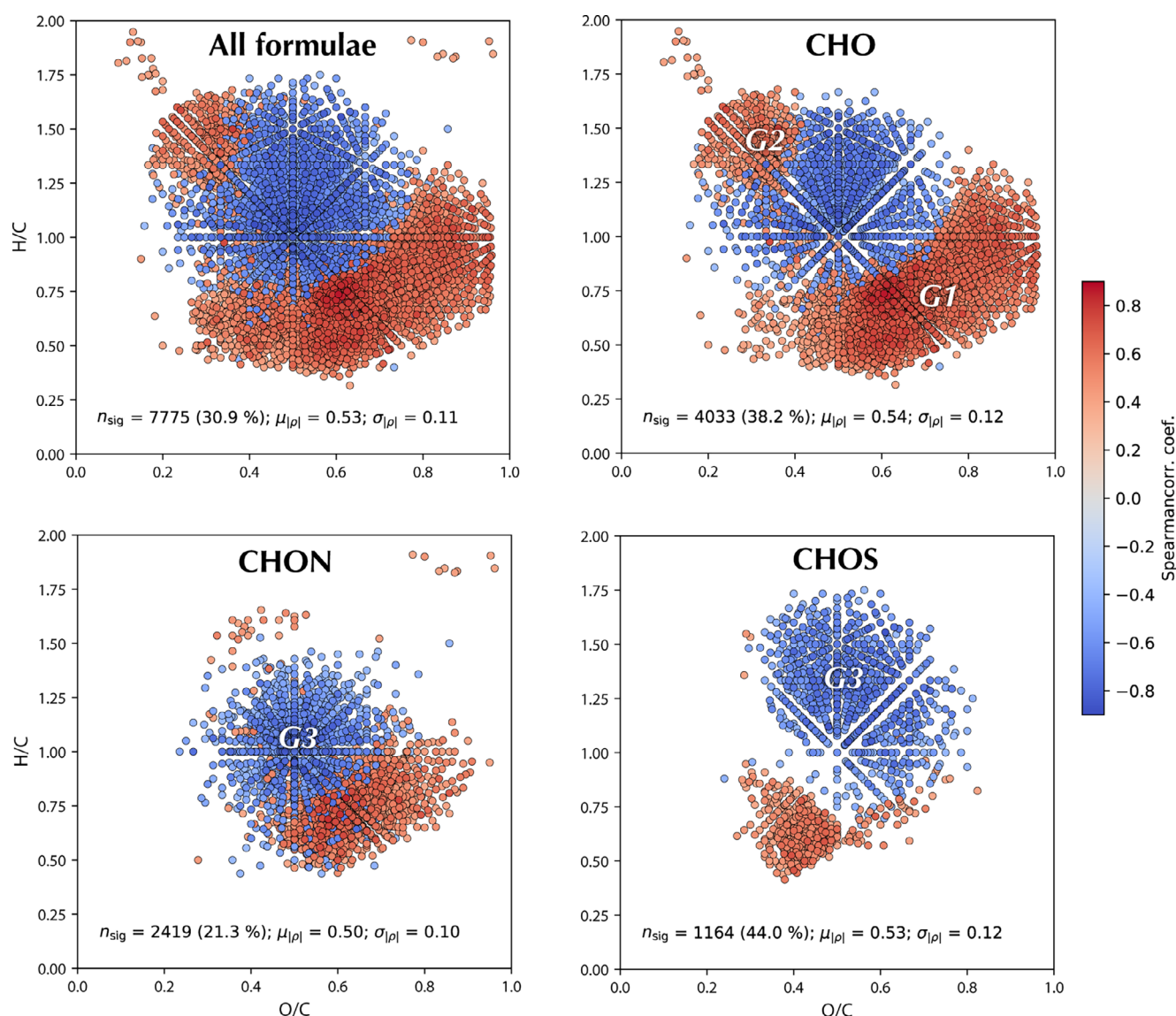

Fig. 8. Spearman rank correlations of relative abundance of molecular formulae derived from negative-ion 21 T ESI FT-ICR MS with river discharge split by heteroatomic class (all, CHO, CHON, and CHOS). Colors represent the correlation coefficient (ρs) between the relative intensity of each molecular formulae and discharge. Red points are more abundant when discharge is high while blue points are more abundant when discharge is low. For each panel the n_{sig} is the number of significantly correlated formulae with the proportion of common formulae comprised by n_{sig} shown in parentheses. The mean (μ) and standard deviation (σ) of the absolute value of $|\rho s|$ for all formulae are also displayed in each panel.

more combustion derived DOM, likely due to inputs from the savanna dominated Kasai River Basin (Drake et al. 2020b).

Despite the observed homogeneity of DOM based on first-order compound classes, it is well known that these broad classifications often fail to capture trends that may exist among individual molecular formulae or groups of formulae that either fall into less abundant compound classes or span multiple compound classes. Using Spearman-rank correlation between discharge (a proxy for seasonality) and the relative abundance of individual molecular formulae to delve beyond the broad compound classes, $\sim 31\%$ of all formulae ($n = 7775$) present in at least half of the samples were found to be significantly ($p < 0.05$) correlated with discharge (Fig. 8). Among these formulae, two distinct clusters composed primarily of CHO-containing formulae were correlated with high discharge: one low H/C, high O/C group (*G1*) and a second smaller group with high H/C and low O/C formulae (*G2*). *G1* is indicative of aromatic vascular plant-derived DOM, which is generally low H/C, high O/C (Stubbins et al. 2010; Kellerman et al. 2018; Spencer et al. 2019). Formulae in the same region as *G2* (H/C of 1.25–1.5 and O/C of 0.3) are often ascribed to lipid-like compounds (D'Andrilli et al. 2015), which can also be derived from terrestrial vegetation. Previous studies that examined DOM composition across multiple tropical catchments have shown similar groups of formulae to be correlated with the extent of forests within a catchment (Drake et al. 2019, 2020a; Spencer et al. 2019).

The spearman-rank correlation also revealed a heteroatomic (i.e., containing N or S) cluster with elevated H/C and moderate O/C ratios (*G3*, Fig. 8) that was negatively correlated with discharge (blue formulae). This negative correlation of N-containing formulae with discharge corresponds well with the observed decrease in C : N ratios of DOM at low discharge (Fig. 7C). Together, the low C : N ratios and relatively more aliphatic (high H/C) and heteroatomic composition indicates an increasing influence of soil OM, which tends to have low aromaticity and higher N content derived from microbial necromass and processed organic matter (Kögel-Knabner et al. 2000; Wilson and Xenopoulos 2008; Kaiser and Kalbitz 2012; Kellerman et al. 2018). The correlation of the "soil-like" *G3* group with base-flow conditions is likely a result of a larger proportion of water flowing through subsurface soils during low flow periods compared to high flow periods. Overall, these spearman-rank correlation results indicate that despite the general seasonal homogeneity and predominance of forest vegetation as a source of DOM in the Ruki River, more nuanced compositional shifts from soil-derived DOM to vascular-plant derived DOM driven by hydrologic flowpaths are still evident.

Conclusion

This year-long study into the C biogeochemistry of the Ruki River revealed a strong hydrologic control over dissolved and particulate C concentrations and export. As a good candidate for being one of the most pristine and homogenous tropical forest watersheds on Earth, the Ruki is the prototypical blackwater river. As with most blackwater rivers, total C in the Ruki was dominated by DOC, the acidity of which likely exerted a titrating effect on DIC, the second largest pool of C. This effect on the carbonate equilibrium resulted in the strong relationship between $p\mathrm{CO}_2$ and discharge, suggesting that increased outgassing of CO_2 from blackwater rivers is facilitated by both physical translocation of soil-derived CO_2 to the river and in-situ chemical shifts in pH caused by higher concentrations of organic acids. Moreover, the increase in DOC with discharge may have also fueled higher rates of respiration, thereby increasing CO_2 concentrations further during peak discharge. The observed DOC yield in the Ruki makes it one of the most efficient exporters of DOC globally, exceeding even the Rio Negro and other well-studied blackwater rivers. Given the Ruki's pristine forested nature and lowland context, erosion and sediment transport were low. The observed negative relationship between POC and discharge along with the high proportion of TSS comprised by POC indicates the lack of mechanical erosion and limited supply of sediments to be mobilized by rainfall. Isotopic ratios of DOC and POC and molecular compositions of DOM unsurprisingly reflect the dominance of modern C3 forest land cover within the Ruki Basin, although minor shifts in ^{13}C-POC, DOM C : N ratio, and the relative intensities of DOM formulae revealed by spearman-rank correlations indicate more nuanced seasonal transitions between material sourced from aboveground vegetation or litter and soil organic matter. In addition to these nuanced compositional shifts, the presence of aged but ^{13}C-depleted DOC during the falling limb of the primary discharge peak points to the possible mobilization of peat-derived OC. Whether this is a normal seasonal phenomenon driven by hydrology or a result of a more isolated disturbance event is unclear and should be resolved by further investigation. Destabilization of ancient OC-rich stores of peat in the Congo Basin, especially in such a pristine context as the Ruki, is a concerning finding given the potential for such a flux to exacerbate the accumulation of CO_2 in the atmosphere. Overall, the C biogeochemistry of the Ruki River renders it a disproportionately large end-member source of forest-derived OC to the Congo River relative to its watershed area and a useful watershed to study the nuanced effects of hydrology and organic chemistry on the downstream flux of C from a highly productive tropical lowland forest ecosystem.

Data availability statement

All data used in the analyses for this manuscript is available in the Ruki_Master.xlsx file available with the online version. All FT-ICR MS data files are publicly available via the Open Science Framework (https://osf.io/nge7k/) at DOI 10.17605/OSF.IO/NGE7K.

References

Abril, G., and others. 2014. Amazon River carbon dioxide outgassing fueled by wetlands. Nature **505**: 395–398.

Battin, T. J., S. Luyssaert, L. A. Kaplan, A. K. Aufdenkampe, A. Richter, and L. J. Tranvik. 2009. The boundless carbon cycle. Nat. Geosci. **2**: 598–600.

Baumgartner, S., and others. 2020. Seasonality, drivers, and isotopic composition of soil CO_2 fluxes from tropical forests of The Congo Basin. Biogeosciences **17**: 6207–6218.

Baumgartner, S., and others. 2022. Fluvial sediment export from pristine forested headwater catchments in The Congo Basin. Geomorphology **398**: 108046.

Behnke, M. I., and others. 2021. Pan-arctic riverine dissolved organic matter: Synchronous molecular stability, shifting sources and subsidies. Global Biogeochem. Cycles **35**: e2020GB006871.

Blakney, G. T., C. L. Hendrickson, and A. G. Marshall. 2011. Predator data station: A fast data acquisition system for advanced FT-ICR MS experiments. Int J Mass Spectr **306**: 246–252.

Borges, A. V., and others. 2015. Globally significant greenhouse-gas emissions from African inland waters. Nat. Geosci. **8**: 637–642.

Borges, A. V., and others. 2019. Variations in dissolved greenhouse gases (CO_2, CH_4, N_2O) in The Congo River network overwhelmingly driven by fluvial-wetland connectivity. Biogeosciences **16**: 3801–3834.

Boström, B., D. Comstedt, and A. Ekblad. 2007. Isotope fractionation and 13C enrichment in soil profiles during the decomposition of soil organic matter. Oecologia **153**: 89–98.

Bouillon, S., A. Yambélé, R. G. M. Spencer, D. P. Gillikin, P. J. Hernes, J. Six, R. Merckx, and A. Borges. 2012. Organic matter sources, fluxes and greenhouse gas exchange in the Oubangui River (Congo River basin). Biogeosciences **9**: 2045–2062.

Bouillon, S., A. Yambélé, D. P. Gillikin, C. Teodoru, F. Darchambeau, T. Lambert, and A. V. Borges. 2014. Contrasting biogeochemical characteristics of the Oubangui River and tributaries (Congo River basin). Sci. Rep. **4**: 5402.

Cook, S., and others. 2018. Fluvial organic carbon fluxes from oil palm plantations on tropical peatland. Biogeosciences **15**: 7435–7450.

Corilo. 2014. PetroOrg software. Florida State University.

Coynel, A., P. T. Seyler, H. Etcheber, M. Meybeck, and D. Orange. 2005. Spatial and seasonal dynamics of total suspended sediment and organic carbon species in The Congo River. Global Biogeochem. Cycles **19**: GB4019.

Crezee, B., and others. 2022. Mapping peat thickness and carbon stocks of the Central Congo Basin using field data. Nat. Geosci. **15**: 639–644.

D'Andrilli, J., W. T. Cooper, C. M. Foreman, and A. G. Marshall. 2015. An ultrahigh-resolution mass spectrometry index to estimate natural organic matter lability. Rapid Commun. Mass Spectrom. **29**: 2385–2401.

Dargie, G. C., S. L. Lewis, I. T. Lawson, E. T. A. Mitchard, S. E. Page, Y. E. Bocko, and S. A. Ifo. 2017. Age, extent and carbon storage of the Central Congo Basin peatland complex. Nature **542**: 86–90.

Dargie, G. C., and others. 2019. Congo Basin peatlands: Threats and conservation priorities. Mitig. Adapt. Strat. Glob. Chang. **24**: 669–686.

Descy, J.-P., F. Darchambeau, T. Lambert, M. P. Stoyneva-Gaertner, S. Bouillon, and A. V. Borges. 2017. Phytoplankton dynamics in the Congo river. Freshw. Biol. **62**: 87–101.

Dornblaser, M. M., and R. G. Striegl. 2009. Suspended sediment and carbonate transport in the Yukon River basin, Alaska: Fluxes and potential future responses to climate change. Water Resour. Res. **45**: 382.

Drake, T. W., F. Guillemette, J. D. Hemingway, J. P. Chanton, D. C. Podgorski, N. S. Zimov, and R. G. M. Spencer. 2018*a*. The ephemeral signature of permafrost carbon in an Arctic fluvial network. J. Geophys. Res. Biogeo. **123**: 1475–1485.

Drake, T. W., P. A. Raymond, and R. G. M. Spencer. 2018*b*. Terrestrial carbon inputs to inland waters: A current synthesis of estimates and uncertainty. Limnol Oceanogr Lett **3**: 132–142.

Drake, T. W., and others. 2019. Mobilization of aged and biolabile soil carbon by tropical deforestation. Nat. Geosci. **12**: 541–546.

Drake, T. W., D. C. Podgorski, B. Dinga, J. P. Chanton, J. Six, and R. G. M. Spencer. 2020*a*. Land-use controls on carbon biogeochemistry in lowland streams of The Congo Basin. Glob. Chang. Biol. **26**: 1374–1389.

Drake, T. W., S. Wagner, A. Stubbins, J. N. Wabakanghanzi, J. B. Dinga, J. Six, and R. G. M. Spencer. 2020*b*. Du feu à l'Eau: Source and flux of dissolved black carbon from The Congo River. Global Biogeochem. Cycles **34**: 1615.

de Fátima, F. L., M. Rasera, A. V. Krusche, J. E. Richey, M. V. R. Ballester, and R. L. Victória. 2013. Spatial and temporal variability of pCO_2 and CO_2 efflux in seven Amazonian Rivers. Biogeochemistry **116**: 241–259.

Fellman, J. B., D. V. D'Amore, and E. Hood. 2008. An evaluation of freezing as a preservation technique for analyzing dissolved organic C, N and P in surface water samples. Sci. Total Environ. **392**: 305–312.

Godsey, S. E., J. W. Kirchner, and D. W. Clow. 2009. Concentration-discharge relationships reflect chemostatic characteristics of US catchments. Hydrol. Process. **23**: 1844–1864.

Gómez-Gener, L., and others. 2021. Global carbon dioxide efflux from rivers enhanced by high nocturnal emissions. Nat. Geosci. **14**: 289–294.

Gonsior, M., and others. 2016. Chemodiversity of dissolved organic matter in the Amazon Basin. Biogeosciences **13**: 4279–4290.

Haghipour, N., B. Ausin, M. O. Usman, N. Ishikawa, L. Wacker, C. Welte, K. Ueda, and T. I. Eglinton. 2019. Compound-specific radiocarbon analysis by elemental analyzer-accelerator

mass spectrometry: Precision and limitations. Anal. Chem. **91**: 2042–2049.

Hemingway, J. D. 2017. Fouriertransform: Open-source tools for FT-ICR MS data analysis.

Hemingway, J. D., E. Schefuß, R. G. M. Spencer, B. J. Dinga, T. I. Eglinton, C. McIntyre, and V. V. Galy. 2017. Hydrologic controls on seasonal and inter-annual variability of Congo River particulate organic matter source and reservoir age. Chem. Geol. **466**: 454–465.

Hendrickson, C. L., J. P. Quinn, N. K. Kaiser, and others. 2015. 21 Tesla Fourier transform ion cyclotron resonance mass spectrometer: A national resource for ultrahigh resolution mass analysis. J. Am. Soc. Mass Spectrom. **26**: 1626–1632.

Hursh, C. R., and E. F. Brater. 1941. Separating storm-hydrographs from small drainage-areas into surface-and subsurface-flow. Transactions, American Geophysical Union.

Jones, A., and others. 2013. Soil atlas of Africa. European Commision.

Kaiser, K., and K. Kalbitz. 2012. Cycling downwards-dissolved organic matter in soils. Soil Biol. Biochem. **52**: 29–32.

Kellerman, A. M., F. Guillemette, D. C. Podgorski, G. R. Aiken, K. D. Butler, and R. G. M. Spencer. 2018. Unifying concepts linking dissolved organic matter composition to persistence in aquatic ecosystems. Environ. Sci. Tech. **52**: 2538–2548.

Koch, B. P., M. Witt, R. Engbrodt, and T. Dittmar. 2005. Molecular formulae of marine and terrigenous dissolved organic matter detected by electrospray ionization Fourier transform ion cyclotron resonance mass spectrometry. Geochem Cosmochim Acta **69**: 3299–3308.

Koch, B. P., and T. Dittmar. 2006. From mass to structure: An aromaticity index for high-resolution mass data of natural organic matter. Rapid Commun. Mass Spectrom. **20**: 926–932.

Koch, B. P., T. Dittmar, M. Witt, and G. Kattner. 2007. Fundamentals of molecular formula assignment to ultra-high resolution mass data of natural organic matter. Anal. Chem. **79**: 1758–1763.

Koch, B. P., and T. Dittmar. 2016. From mass to structure: An aromaticity index for high-resolution mass data of natural organic matter [correction]. Rapid Commun. Mass Spectrom. **30**: 250.

Kögel-Knabner, I., K. U. Totsche, and B. Raber. 2000. Desorption of polycyclic aromatic hydrocarbons from soil in the presence of dissolved organic matter: Effect of solution composition and aging. J. Environ. Qual. **29**: 906–916.

Kurek, M. R., and others. 2021. Drivers of organic molecular signatures in the Amazon River. Global Biogeochem. Cycles **35**: 1–16.

Kurek, M. R., and others. 2022. Organic molecular signatures of The Congo river and comparison to the Amazon. Global Biogeochem. Cycles **36**: e2022GB007301.

Lambert, T., S. Bouillon, F. Darchambeau, P. Massicotte, and A. V. Borges. 2016. Shift in the chemical composition of dissolved organic matter in The Congo River network. Biogeosciences **13**: 5405–5420.

Mann, P. J., R. G. M. Spencer, and B. J. Dinga. 2014. The biogeochemistry of carbon across a gradient of streams and rivers within The Congo Basin. J Geophys Res Biogeochem **119**: 687–702.

Marwick, T. R., F. Tamooh, C. R. Teodoru, A. V. Borges, F. Darchambeau, and S. Bouillon. 2015. The age of river-transported carbon: A global perspective. Global Biogeochem. Cycles **29**: 122–137.

Maurice, R. 1947. Le Congo Physique. H. Vaillant-Carmanne.

Mcintyre, C. P., L. Wacker, N. Haghipour, T. M. Blattmann, S. Fahrni, M. Usman, T. I. Eglinton, and H.-A. Synal. 2017. Online 13C and 14C gas measurements by EA-IRMS–AMS at ETH Zürich. Radiocarbon **59**: 893–903.

Meybeck, M. 1982. Carbon, nitrogen, and phosphorus transport by world rivers. Am. J. Sci. **282**: 401–450.

Meybeck, M., and A. Ragu. 1997. River discharges to the oceans: An assessment of suspended solids, major ions and nutrients. UNEP.

Moore, S., and others. 2013. Deep instability of deforested tropical peatlands revealed by fluvial organic carbon fluxes. Nature **493**: 660–663.

Moreira-Turcq, P., P. T. Seyler, J. L. Guyot, and H. Etcheber. 2003. Exportation of organic carbon from the Amazon River and its main tributaries. Hydrol. Process. **17**: 1329–1344.

Musolff, A., C. Schmidt, B. Selle, and J. H. Fleckenstein. 2015. Catchment controls on solute export. Adv. Water Resour. **86**: 133–146.

Paolini, J., R. Hevia, and R. Herrera. 1987. Transport of carbon and minerals in the Orinoco and Caroni rivers during the years 1983–1984. Mitteilungen aus dem Geologisch-Paläontologischen Institut der Universität Hamburg **64**: 325–338.

Pérez, M. A. P., P. Moreira-Turcq, H. Gallard, T. Allard, and M. F. Benedetti. 2011. Dissolved organic matter dynamic in the Amazon basin: Sorption by mineral surfaces. Chem. Geol. **286**: 158–168.

Raymond, P. A., and J. E. Bauer. 2001. Use of 14C and 13C natural abundances for evaluating riverine, estuarine, and coastal DOC and POC sources and cycling: A review and synthesis. Org. Geochem. **32**: 469–485.

Raymond, P. A., and R. G. M. Spencer. 2015. Chapter 11–riverine DOM, p. 509–533. *In* D. A. Hansell and C. A. Carlson [eds.], Biogeochemistry of marine dissolved organic matter, 2nd ed. Academic Press.

Raymond, P. A., and others. 2012. Scaling the gas transfer velocity and hydraulic geometry in streams and small rivers. Limnol. Oceanogr. **2**: 41–53.

Richey, J. E., J. I. Hedges, A. H. Devol, P. D. Quay, R. Victoria, L. Martinelli, and B. R. Forsberg. 1990. Biogeochemistry of carbon in the Amazon River. Limnol. Oceanogr. **35**: 352–371.

Richey, J. E., J. M. Melack, A. K. Aufdenkampe, V. M. Ballester, and L. L. Hess. 2002. Outgassing from Amazonian rivers and wetlands as a large tropical source of atmospheric CO2. Nature **416**: 617–620.

Rose, L. A., D. L. Karwan, and S. E. Godsey. 2018. Concentration–discharge relationships describe solute and sediment mobilization, reaction, and transport at event and longer timescales. Hydrol Process **32**: 2829–2844.

Runge, J. 2008. The Congo River, Central Africa. Large Rivers: Geomorphology and Management. Chichester, John Wiley and Sons Ltd, p. 293–309.

Runkel, R. L., C. G. Crawford, and T. A. Cohn. 2004. Load Estimator (LOADEST): A FORTRAN program for estimating constituent loads in streams and rivers: U.S. Geological Survey Techniques and Methods Book 4, Chapter A5, p. 69.

Šantl-Temkiv, T., K. Finster, T. Dittmar, B. M. Hansen, R. Thyrhaug, N. W. Nielsen, and U. G. Karlson. 2013. Hailstones: A window into the microbial and chemical inventory of a storm cloud. PloS One **8**: e53550.

Savory, J. J., N. K. Kaiser, A. M. McKenna, F. Xian, G. T. Blakney, R. P. Rodgers, C. L. Hendrickson, and A. G. Marshall. 2011. Parts-per-billion Fourier transform ion cyclotron resonance mass measurement accuracy with a "walking" calibration equation. Anal. Chem. **83**: 1732–1736.

Seyler, P. T., and others. 2005. Organic carbon transported by the equatorial rivers: Example of Congo-Zaire and Amazon basins. Soil Erosion and Carbon Dynamics. CRC Press, p. 275–288.

Smith, D. F., D. C. Podgorski, R. P. Rodgers, G. T. Blakney, and C. L. Hendrickson. 2018. 21 Tesla FT-ICR mass spectrometer for ultrahigh-resolution analysis of complex organic mixtures. Anal. Chem. **90**: 2041–2047.

Spencer, R. G. M., P. J. Hernes, R. Ruf, A. Baker, R. Y. Dyda, A. Stubbins, and J. Six. 2010. Temporal controls on dissolved organic matter and lignin biogeochemistry in a pristine tropical river, Democratic Republic of Congo. J. Geophys. Res. **115**: 2069.

Spencer, R. G. M., and others. 2012. An initial investigation into the organic matter biogeochemistry of The Congo River. Geochim. Cosmochim. Acta **84**: 614–627.

Spencer, R. G. M., P. J. Hernes, and B. Dinga. 2016. Origins, seasonality, and fluxes of organic matter in The Congo River. Global Biogeochem. Cycles **30**: 1105–1121.

Spencer, R. G. M., A. M. Kellerman, D. C. Podgorski, M. N. Macedo, K. Jankowski, D. Nunes, and C. Neill. 2019. Identifying the molecular signatures of agricultural expansion in Amazonian headwater streams. J. Geophys. Res. Biogeo. **124**: 1637–1650.

Stubbins, A., and others. 2010. Illuminated darkness: Molecular signatures of Congo River dissolved organic matter and its photochemical alteration as revealed by ultrahigh precision mass spectrometry. Limnol. Oceanogr. **55**: 1467–1477.

Stuiver, M., and H. A. Polach. 1977. Discussion reporting of 14 C data. Radiocarbon **19**: 355–363.

Terzer-Wassmuth, S., L. I. Wassenaar, J. M. Welker, and L. J. Araguás-Araguás. 2021. Improved high-resolution global and regionalized isoscapes of δ 18 O, δ 2 H and d -excess in precipitation. Hydrol Process **35**: 1–13.

Upstill-Goddard, R., M. Salter, P. J. Mann, J. Barnes, J. Poulsen, B. Dinga, G. Fiske, and R. Holmes. 2017. The riverine source of CH4 and N2O from the republic of Congo, western Congo Basin. Biogeosciences **14**: 2267–2281.

Wacker, L., and others. 2010. MICADAS: Routine and high-precision radiocarbon dating. Radiocarbon **52**: 252–262.

Wagner, S., T. Riedel, J. Niggemann, A. V. Vähätalo, T. Dittmar, and R. Jaffé. 2015. Linking the molecular signature of heteroatomic dissolved organic matter to watershed characteristics in world Rivers. Environ. Sci. Tech. **49**: 13798–13806.

Wang, Z. A., D. J. Bienvenu, P. J. Mann, K. A. Hoering, J. R. Poulsen, R. G. M. Spencer, and R. M. Holmes. 2013. Inorganic carbon speciation and fluxes in The Congo River. Geophys. Res. Lett. **40**: 511–516.

Werner, R. A., B. A. Bruch, and W. A. Brand. 1999. ConFlo III - an interface for high precision delta(13)C and delta(15) N analysis with an extended dynamic range. Rapid Commun. Mass Spectrom. **13**: 1237–1241.

Werner, R. A., and W. A. Brand. 2001. Referencing strategies and techniques in stable isotope ratio analysis. Rapid Commun. Mass Spectrom. **15**: 501–519.

Wilson, H. F., and M. A. Xenopoulos. 2008. Effects of agricultural land use on the composition of fluvial dissolved organic matter. Nat. Geosci. **2**: 37–41.

Xian, F., C. L. Hendrickson, G. T. Blakney, S. C. Beu, and A. G. Marshall. 2010. Automated broadband phase correction of Fourier transform ion cyclotron resonance mass spectra. Anal. Chem. **82**: 8807–8812.

Acknowledgments

Conflict of Interest

None declared.